

# Deep Learning in Random Neural Fields: Numerical Experiments via Neural Tangent Kernel

Kaito Watanabe<sup>1</sup>, Kotaro Sakamoto<sup>2</sup>, Ryo Karakida<sup>3</sup>, Sho Sonoda<sup>4</sup>, Shun-ichi Amari<sup>5,6,7</sup>

<sup>1</sup>University of Tsukuba, Japan

<sup>2</sup>The Institute of Statistical Mathematics, Japan

<sup>3</sup>AIST, Japan

<sup>4</sup>RIKEN AIP, Japan

<sup>5</sup>RIKEN CBS, Japan

<sup>6</sup>ACRO, Teikyo University, Japan

<sup>7</sup>Araya Inc, Japan

February 11, 2022

## Abstract

A biological neural network in the cortex forms a neural field. Neurons in the field have their own receptive fields, and connection weights between two neurons are random but highly correlated when they are in close proximity in receptive fields. In this paper, we investigate such neural fields in a multilayer architecture to investigate the supervised learning of the fields. We empirically compare the performances of our field model with those of randomly connected deep networks. The behavior of a randomly connected network is investigated on the basis of the key idea of the neural tangent kernel regime, a recent development in the machine learning theory of over-parameterized networks; for most randomly connected neural networks, it is shown that global minima always exist in their small neighborhoods. We numerically show that this claim also holds for our neural fields. In more detail, our model has two structures: i) each neuron in a field has a continuously distributed receptive field, and ii) the initial connection weights are random but not independent, having correlations when the positions of neurons are close in each layer. We show that such a multilayer neural field is more robust than conventional models when input patterns are deformed by noise disturbances. Moreover, its generalization ability can be slightly superior to that of conventional models.

## 1 Introduction

Neural networks in the brain cortex have been optimized to perform intelligent information processing throughout their long evolutionary history. The aim of theoretical neuroscience is to understand the complex dynamics of neural networks such as pattern formation [1], self-organized feature extraction [2], and topographic organization [3]. Complex dynamics of neural networks have been studied by using two types of models: random models and field models. The random model is a neural network model with random connections. Theoretical analyses of this model are known as statistical neurodynamics or mean field theory, and they have enabled us to understand the complicated dynamics of neural networks through macroscopic parameters [4–13]. Random models are also used in practical applications, for example, the echo state network in reservoir computing [14]. On the

other hand, in a neural field, neurons form a continuous field, capturing the structure of the cortex, which consists of layered sheets of densely aligned neurons [1–3, 15–23].

While these theoretical models have shed light into the firing dynamics of neural networks, it has been unclear how they can be combined with problems of learning. In particular, there have been few studies on the supervised learning of neural fields [24]. Recently, however, in the literature of deep learning, studies on the *neural tangent kernel (NTK)* [25] have revealed that the random model can achieve zero training error and a high generalization performance with a sufficiently small change in parameters. NTK research has shown that the global optimum for a given set of training examples is always found in a small neighborhood of randomly assigned initial connections [25, 26]. Within the NTK regime, a number of studies have shed light on the global convergence and generalization properties of sufficiently wide neural networks [27–38]. From this, we can expect that if the neural field model can be merged with the random model, we can formulate the supervised learning of the neural field through the NTK framework.

Inspired by these trends of research, we investigate the robustness and generalization ability of multilayer neural fields in supervised learning tasks. Our model of multilayer neural fields has a correlated initial random structure of neural connections in which each neuron has a continuous receptive field. A typical deep neural network model does not use correlations among initial connections. It is physiologically known that the activities of neighboring neurons are correlated [39]. Mathematically, this means reduction in the size of the reproducing kernel Hilbert space (RKHS). It is known that the generalization performance can be improved by reducing the RKHS [40]. Thus, we implement these structures with continuously distributed receptive fields by introducing weights depending on the distances between neurons and random initial connection weights that are not statistically independent but have correlations depending on the positions of the neurons in neural fields. In the case of no correlations and sufficiently large receptive fields, our model simply reduces to a conventional multilayer neural network.

In the present paper, we first formulate our model mathematically. Next, we address three research questions: (1) How do the performances of neural fields depend on the intensity of the correlation in the initial random connections and also the size of the receptive field? (2) Are neural fields with correlated neurons and receptive fields still governed by the NTK regime? (3) Does our model improve robustness to perturbations? We aim to investigate these questions with numerical simulations, although the simulations are preliminary.

**Contributions.** The main results in the present paper are as follows.

- We formulate and investigate the supervised learning of multilayer random neural fields. We numerically confirm that our model of multilayer random neural fields with correlated neurons and receptive fields is governed by the NTK regime.
- We find that our model of random neural fields is robust under the disturbances of both random noise and deformation of training samples. The generalization ability is slightly superior to those of conventional models of neural networks.

## 2 Random Neural Fields

For simplicity, we assume periodic boundary conditions on a one-dimensional neural field. Namely, the field is on a torus  $\mathbb{T} := \mathbb{R}/T\mathbb{Z}$  with period  $T$  identified with  $[-T/2, T/2]$ . This setting is widely used in the study of neural fields [3, 41, 42] and improves the mathematical outlook.

## 2.1 Formulation

We formulate a  $d$ -dimensional random neural field ( $d$ -RNF). Typically,  $d = 2$  for image processing. The positions of neurons in the  $l$ th layer are denoted by  $\mathbf{z}_l \in \mathbb{T}^d$ . The behavior of the model is described as

$$\begin{cases} h^l(\mathbf{z}_l) &= \int_{\mathbb{T}^d} w^l(\mathbf{z}_l, \mathbf{z}_{l-1}) x^{l-1}(\mathbf{z}_{l-1}) d\mathbf{z}_{l-1} + b^l(\mathbf{z}_l) \\ x^l(\mathbf{z}_l) &= \varphi(h^l(\mathbf{z}_l)), \end{cases} \quad (1)$$

where  $w^l(\mathbf{z}_l, \mathbf{z}_{l-1})$  is a scalar weight connecting a neuron at position  $\mathbf{z}_{l-1}$  in the  $(l-1)$ -th layer to a neuron at position  $\mathbf{z}_l$  in the  $l$ th layer,  $h^l(\mathbf{z}^l)$  is the pre-activation of the neuron at  $\mathbf{z}_l$ ,  $b^l(\mathbf{z}_l)$  is a bias function, and  $x^l(\mathbf{z}_l)$  is the output of this neuron, which becomes the input to the next  $(l+1)$ -th layer. Here,  $\varphi(\cdot)$  is an activation function.

The final output  $y \in \mathbb{R}$  is a scalar that is a linear function of the outputs of the final layer  $L$  of the neural field for input  $\mathbf{x} = \mathbf{x}^0$ ,

$$y = f(\mathbf{x}, \theta) = \int_{\mathbb{T}^d} w^{L+1}(\mathbf{z}_L) x^L(\mathbf{z}_L) d\mathbf{z}_L. \quad (2)$$

We denote by vector  $\theta$  the set of all parameters:  $\theta = \{\tilde{w}^l(\cdot, \cdot), b^l(\cdot); l = 1, \dots, L+1\}$ .

The initial weights and biases are distributed according to a Gaussian process as  $\mathcal{GP}(0, K)$  and  $\mathcal{GP}(0, K_b)$  with mean zero and covariance function  $K$  and  $K_b$  depending on the positions of neurons in the  $(l-1)$ -th and  $l$ -th layers, as

$$\begin{cases} \tilde{w}^l(\mathbf{z}_l, \mathbf{z}_{l-1}) \sim \mathcal{GP}(0, K), \\ b^l(\mathbf{z}_l) \sim \mathcal{GP}(0, K_b). \end{cases} \quad (3)$$

In the other words,  $\tilde{w}^l(\mathbf{z}_l, \mathbf{z}_{l-1})$  are Gaussian random variables with mean 0 and covariance  $K(|\mathbf{z}_l - \mathbf{z}'_l|, |\hat{\mathbf{z}}_l - \hat{\mathbf{z}}'_{l-1}|)$ . We may assume, for simplicity, that  $\tilde{w}^l(\mathbf{z}_l, \mathbf{z}'_{l-1})$  and  $\tilde{w}^l(\hat{\mathbf{z}}_l, \hat{\mathbf{z}}'_{l-1})$  are statistically independent when  $\mathbf{z}_l \neq \hat{\mathbf{z}}_l$ . That is, different neurons are not correlated. Fig. 1 shows the relation between RNF output and random field. Darker lines depict neurons closer to  $\hat{\mathbf{z}}_{l-1}$  which have a higher correlation. The blue line represents the output  $x^l(\mathbf{z}_l)$ . We also introduce receptive fields to the random field as will be described in Section 2.2. The connection weights of  $\tilde{w}^l(\mathbf{z}_l, \mathbf{z}'_{l-1})$  and  $\tilde{w}^l(\hat{\mathbf{z}}_l, \hat{\mathbf{z}}'_{l-1})$  have covariance given by  $K(|\hat{\mathbf{z}}_{l-1} - \mathbf{z}'_{l-1}|)$ . A simple example is Gaussian

$$K(|\hat{\mathbf{z}}_{l-1} - \mathbf{z}'_{l-1}|) = \exp\left(-\frac{|\hat{\mathbf{z}}_{l-1} - \mathbf{z}'_{l-1}|^2}{2\sigma^2}\right). \quad (4)$$

In addition, as a covariance function, we will also use a Matérn kernel and an RBF kernel on the  $d$ -dimensional torus  $\mathbb{T}^d$ . Their detailed formulations are described in A.

Since the Matérn kernel is a parameterized family of distributions that covers a variety of distributions from Gaussian to Student  $t$  and Cauchy, it is convenient to examine the effect of different strengths of correlation in the receptive field. The Matérn kernel is preferable because the corresponding RKHS is a Sobolev space, where the parameter corresponds to the smoothness. Namely, the parameter controls the complexity of the hypothesis class and thus the RKHS is a natural hypothesis space.

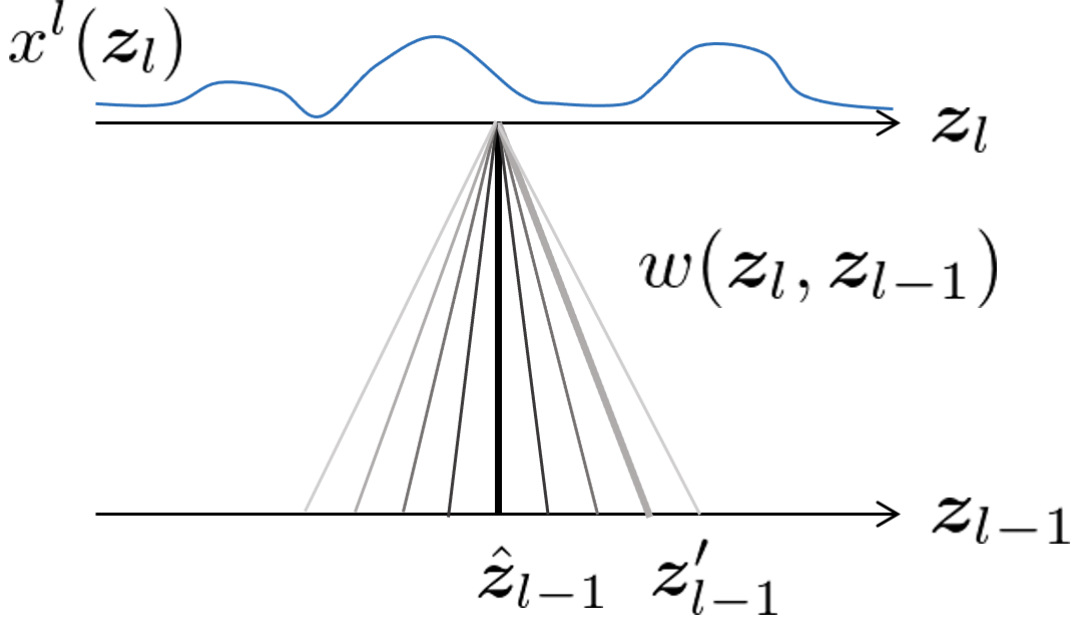


Figure 1: Relation between RNF output and random field.

Table 1: Receptive fields.

Name	Definition
Gaussian filter	$r(z_l, z_{l-1}) = \exp\left(-\frac{ z_l - z_{l-1} ^2}{2\sigma_r^2}\right)$
Mexican hat	$r(z_l, z_{l-1}) = \frac{2}{\sqrt{3\sigma_r}\pi^{1/4}} \left(1 - \left(\frac{ z_l - z_{l-1} }{\sigma_r}\right)^2\right) \exp\left(-\frac{ z_l - z_{l-1} ^2}{2\sigma_r^2}\right)$

## 2.2 Neural fields with receptive fields

Let  $r^l(z_l, z_{l-1})$  denote the receptive field of a neuron at position  $z_l$  of the  $l$ th layer such that  $r^l(z_l, z_{l-1}) = 0$  when neurons at  $z_{l-1}$  of the  $(l-1)$ -th layer are outside the receptive field of the neuron at  $z_l$ . We introduce the connection weights as  $w(z_l, z_{l-1}) = \tilde{w}(z_l, z_{l-1})r^l(z_l, z_{l-1})$  by using the  $\tilde{w}$  of the Gaussian field of (3). In addition to the Gaussian receptive field, we also consider the Mexican-hat-type receptive field, which is a typical feature of the receptive fields in the biological brain [43] and also image processing. We define the receptive fields as in Tab. 1.

## 2.3 Convolutional neural networks

Our model can be easily applied to convolutional neural networks (CNN). From the canonical representation of the Gaussian process [44], correlated Gaussian fields  $w \sim \mathcal{GP}(0, K)$  with covariance function  $K$  can be expressed using an appropriate spectral density  $f$  as

$$w(\mathbf{t})\sqrt{d\mathbf{t}} = \int_{\mathbb{T}^d} f(\mathbf{t} - \mathbf{s})dB(\mathbf{s}), \quad (5)$$

where  $\mathbf{t} \in \mathbb{T}^d$  is a vector and  $B(\mathbf{s})$  is a  $d$ -dimensional Wiener process [44]. Using Eq.(5), the  $d$ -RNF can be described as

$$h(\mathbf{u}) = \int_{\mathbb{T}^d} w(\mathbf{t} - \mathbf{u}) x(\mathbf{t}) \sqrt{d\mathbf{t}} = \int_{\mathbb{T}^d} (f \star x)(\mathbf{1}_d - \mathbf{s}, \mathbf{u}) dB(\mathbf{s}), \quad (6)$$

where  $\mathbf{1}_d$  is a  $d$ -dimensional one vector  $(1, 1, \dots, 1) \in \mathbb{R}^d$ , a periodic boundary condition  $x(\mathbf{t}) = x(\mathbf{t} + \mathbf{1}_d)$  is assumed, and

$$f \star x(\mathbf{s}, \mathbf{u}) := \int_{\mathbb{T}^d} f(\mathbf{t}, \mathbf{u}) x(\mathbf{t} + \mathbf{s}) d\mathbf{t}. \quad (7)$$

In this case, the effect of  $K$  is aggregated to  $f \star x$ , which is formally a CNN. That is, the analysis of the  $d$ -RNF reduces to the analysis of the CNN. However, white noise is not differentiable everywhere. Thus, the convolution is not well-defined. In this paper, we consider the justification for the use of white noise to be the generalized functional theory of infinite variables (see B).

### 3 Neural Tangent Kernel

In this section, we describe the neural tangent kernel (NTK), which can capture the learning behavior in a fully connected neural network (FCNN). For input  $\mathbf{x} \in \mathbb{R}^m$ , let  $f_t(\cdot, \boldsymbol{\theta}^t) : \mathbb{R}^m \rightarrow \mathbb{R}$  be the output of the neural network at training step  $t$ , where all the parameters of the network are summarized to  $\boldsymbol{\theta}^t \in \mathbb{R}^P$  ( $P = \sum_{l=0}^{L-1} (n_l + 1)n_{l+1}$ ). For a given training dataset  $\{(\mathbf{x}_i, y_i)\}_{i=1}^N$ , supervised learning is carried out to minimize the mean squared error (MSE) loss. For the two inputs  $\mathbf{x}_i$  and  $\mathbf{x}_j$ , the NTK  $\hat{\Theta}_t(\cdot, \cdot) : \mathbb{R}^m \times \mathbb{R}^m \rightarrow \mathbb{R}$  at training step  $t$  is defined by

$$\hat{\Theta}_t(\mathbf{x}_i, \mathbf{x}_j) := \sum_{k=1}^P \frac{\partial f_t(\mathbf{x}_i, \boldsymbol{\theta}^t)}{\partial \theta_k^t} \frac{\partial f_t(\mathbf{x}_j, \boldsymbol{\theta}^t)}{\partial \theta_k^t}. \quad (8)$$

It is known that NTK at any training step  $t$  can be approximated by the initial random kernel  $\hat{\Theta}_0$ , provided the width of the network is sufficiently large [25, 32]. If  $f_t(\mathcal{X})$  is  $\text{vec}(f_t(\mathbf{x}_1), \dots, f_t(\mathbf{x}_N)) \in \mathbb{R}^N$ , the vector of the concatenated outputs of the network, then NTK  $\hat{\Theta}_t$  is an  $N \times N$  matrix.

The first-order approximation of the output  $f_t(\mathbf{x}_i, \boldsymbol{\theta}^t)$  of the network using Taylor expansion at  $\boldsymbol{\theta}^0$  gives the following equation:

$$f_t(\mathbf{x}_i, \boldsymbol{\theta}^t) \approx f_0(\mathbf{x}_i, \boldsymbol{\theta}^0) + \left\langle \boldsymbol{\theta}^t - \boldsymbol{\theta}^0, \frac{\partial f_0(\mathbf{x}_i, \boldsymbol{\theta}^0)}{\partial \boldsymbol{\theta}^t} \right\rangle. \quad (9)$$

Denoting  $\mathcal{Y} = (y_1, \dots, y_N)^\top \in \mathbb{R}^N$ , we can linearize the above equation into the following equation using NTK  $\hat{\Theta}_0$  in a sufficiently over-parameterized case, i.e.,  $P \gg N$ :

$$f_t(\mathbf{x}') = f_0(\mathbf{x}') - \hat{\Theta}_0(\mathbf{x}', \mathcal{X}) \hat{\Theta}_0^{-1} \left( I - \exp \left( -\eta N^{-1} \hat{\Theta}_0 t \right) \right) (f_0(\mathcal{X}) - \mathcal{Y}), \quad (10)$$

where  $\eta$  is the learning rate. Setting this learning rate  $\eta$  appropriately, output dynamics are perfectly fit with those by backpropagation.

[45] attempted to control various RKHS functions by investigating their smoothness and stability with respect to the deformation and translation of NTK mappings for multilayer networks and CNNs. The average relative distance from the reference image  $\mathbf{x}$  to a deformed image  $\mathbf{x}'$  is obtained by applying the following equation:

$$\frac{1}{|S|} \sum_{\mathbf{x}' \in S} \frac{\|\Phi(\mathbf{x}') - \Phi(\mathbf{x})\|_{\mathcal{H}}}{\|\Phi(\mathbf{x})\|_{\mathcal{H}}} = \frac{1}{|S|} \sum_{\mathbf{x}' \in S} \frac{\sqrt{\hat{\Theta}_0(\mathbf{x}, \mathbf{x}) + \hat{\Theta}_0(\mathbf{x}', \mathbf{x}') - 2\hat{\Theta}_0(\mathbf{x}, \mathbf{x}')}}{\sqrt{\hat{\Theta}_0(\mathbf{x}, \mathbf{x})}}, \quad (11)$$

Table 2: Receptive fields in the discretized case.

Name	Definition
Gaussian filter	$r_{ij}^l = \exp\left(-\frac{1}{2}\left \frac{1}{\sigma_r}\left(\frac{i}{n_l} - \frac{j}{n_{l-1}}\right)\right ^2\right)$ , $i = 1, \dots, n_l$ , $j = 1, \dots, n_{l-1}$
Mexican hat	$r_{ij}^l = \frac{2}{\sqrt{3\sigma_r}\pi^{1/4}}\left(1 - \left \frac{1}{\sigma_r}\left(\frac{i}{n_l} - \frac{j}{n_{l-1}}\right)\right ^2\right)\exp\left(-\frac{1}{2}\left \frac{1}{\sigma_r}\left(\frac{i}{n_l} - \frac{j}{n_{l-1}}\right)\right ^2\right)$

where  $S$  is a set of images,  $\mathcal{H}$  is the RKHS associated with the kernel  $\hat{\Theta}_0$ , and  $\Phi$  is the kernel mapping.

## 4 Experimental Setup

In this section, we describe the setup for preliminary experiments. The code for reproducing our experiments is found in <https://github.com/kwignb/RandomNeuralField>. We used three hidden layer RNF models with an ReLU activation function, and the layer width was 2,048. Stochastic gradient descent (SGD) was used as the optimization method, and the learning rate was  $\eta = 2\lambda_{\max}(\hat{\Theta}_0)^{-1}$ , where  $\lambda_{\max}(\hat{\Theta}_0)$  was the maximum eigenvalue of the NTK. The number of learning epochs was 1,000,000 in the discrete time steps. To reduce the computational cost, 80 training and 20 validation samples were randomly chosen from the MNIST dataset [46]. Instead of solving a classification task, models were trained to classify digits using regression. For the labels of classes  $c \in \{1, \dots, 10\}$ , we defined  $y = -0.1 \cdot \mathbf{1} + \mathbf{e}_c$ , where  $\mathbf{e}_c = (0, \dots, 1, \dots, 0) \in \mathbb{R}^{|c|}$  [47] is the vector in which the  $c$ th component is 1 and the other components are 0. To investigate the robustness of the RNF model to perturbations, we conducted experiments using the infinite MNIST dataset [48].

### 4.1 Discretization

For numerical simulations, we define a discretized RNF model as:

$$\begin{cases} h^l = x^{l-1}W^l + \mathbf{b}^l \\ x^l = \varphi(h^l) \end{cases} \text{ and } \begin{cases} W_{ij}^l = \frac{\sigma_w}{\sqrt{n_l}}r_{ij}^l\tilde{W}_{ij}^{l-1}, \\ b_j^l = \sigma_b\beta_j^l \end{cases} \quad (12)$$

where  $\varphi$  is the ReLU activation function,  $W^l \in \mathbb{R}^{n_{l-1} \times n_l}$  and  $\mathbf{b}^l \in \mathbb{R}^{n_l}$  are weight matrix and bias vectors, respectively,  $r_{ij}^l$  is the receptive field, and  $\beta_j^l$  is generated from the standard Gaussian distribution  $\mathcal{N}(0, 1)$  at initialization. The  $j$ th vector  $\tilde{\mathbf{w}}_j^l$  is generated as:

$$\tilde{\mathbf{w}}_j^l \sim \mathcal{N}(\mathbf{0}_{n_l}, \Sigma^l), \quad \Sigma_{ii'}^l = \exp\left(-\frac{|i - i'|^2}{2(\sigma_{s_l}n_l)^2}\right) \quad (13)$$

where  $\mathbf{0}_{n_{l-1}}$  is an  $n_{l-1}$ -dimensional zero vector. This is the discretization for the Gaussian kernel. See C for the discretization in the case of the Matérn kernel. The receptive fields in the discretized case are shown in Tab. 2.

### 4.2 Correlations

To generate a sample  $\tilde{W}^l$  of the Gaussian random field with mean 0 and covariance  $\Sigma$ , we use the following proposition.

**Proposition 1.** Suppose  $Y = (Y_1, \dots, Y_d)^T \sim \mathcal{N}(\mathbf{0}_d, I_d)$ . For an arbitrary nondegenerate matrix  $A \in \mathbb{R}^{d \times d}$ , let  $X := AY$ . Then,  $X \sim \mathcal{N}(\mathbf{0}_d, AA^T)$ .

First, we calculate the decomposition  $\Sigma^{l-1} = A^{l-1}A^{l-1\top}$ , which is explained later, using the nondegenerate matrix  $A^{l-1}$ . Next, let  $\omega_i^{l-1} \sim \mathcal{N}(\mathbf{0}_{n_{l-1}}, I_{n_{l-1}})$  and  $\tilde{W}^l := \frac{\sigma_w}{\sqrt{n_l}} R^l \circ (A^{l-1}\Omega^l)$ , where  $\circ$  is the Hadamard product,  $R_{ij}^l = r_{ij}^l$ , and  $\Omega^l = (\omega_1^l, \dots, \omega_{n_l}^l) \in \mathbb{R}^{n_{l-1} \times n_l}$ . Then, by the proposition,  $\tilde{W}^l$  is a  $d$ -dimensional realization of the random field.

We remark that the decomposition of  $\Sigma^{l-1}$  is not unique. The Cholesky decomposition is a versatile method for an arbitrary positive definite matrix. However, in implementation, the numerical computation of this decomposition can be time-consuming because  $\Sigma^{l-1}$  tends to have a large dimension. Therefore, in this study, we prepare closed-form formulas to compute  $A^{l-1}$  by using Fourier calculus. See C for concrete equations.

### 4.3 Considered models

We considered five models, Models 1–5, with different structures of initial weights (Tab. 3). In this preliminary study, only the first layer was a neural field with receptive fields and correlated connections. For other layers, the receptive fields were set to be sufficiently wide, and the correlations were set to zero.

Model 1 was a basic RNF. Model 2 acquired the frequency selectivity and translational invariance of CNNs by using random weights and pooling in the second layer [49]. Model 3 was prepared for mimicking the visual cortex. We are interested in how lateral inhibition functions in a feedforward network work. Visual information is processed as retina  $\rightarrow$  LGN (lateral geniculate nucleus)  $\rightarrow$  V1 (primary visual cortex). Mexican-hat-type center-surround inhibitory connections are abundant in an LGN, and a Gabor filter with directionally selective inhibition plays the main role in V1. A linear combination of Mexican-hat-type filters acts as a Gabor filter. NTK cannot extract features, so a hand-crafted filter is used in the first hidden layer to efficiently embed an effective basis that represents images into a kernel.

A fourth model, Model 4, which had a Matérn kernel, was also prepared. The Matérn kernel has a smoothness parameter  $\nu$  that controls the size of the RKHS. The Laplacian kernel can be produced by letting  $\nu = 0.5$ , or the Gaussian kernel can be obtained by letting  $\nu = \infty$ . The supervised learning behavior of RNF models was compared with that of the NTK vanilla model, which is a three-layer network with NTK parameterization (Model 5).

We summarize the evaluated model architectures in Tab. 3, and examples of the generated initial weights are presented in Fig. 5 in D.1. A fully connected layer is denoted as FC layer, where the weights are assumed to be generated independently from the same distribution as in NTK parameterization. When a receptive field is added, it is denoted as (*receptive field*) FC layer, and when the generation method is changed, it is denoted as FC layer (*generation method*).

## 5 Results

In this section, we give the results of several experiments based on the setup described in Section 4.

### 5.1 Random neural fields in NTK regime

In this section, we show by numerical experiments that neural fields follow the NTK regime (Fig. 2). We confirm that the other models are also in the NTK regime (see D.2). The parameters  $\sigma_r$  and  $\sigma_s$  used in these experiments were selected from the combination that minimizes the test loss obtained by NTK regression [25] as described below.

Table 3: Models with three hidden layers: GF=Gaussian filter, MH=Mexican hat, GK=Gaussian kernel, FC= fully connected, and MK=Matérn kernel.

Name	Definition
Model 1	(GF) FC layer (GK) $\rightarrow$ FC layer $\rightarrow$ FC layer
Model 2	(GF) FC layer (GK) $\rightarrow$ MaxPooling $\rightarrow$ FC layer
Model 3	(MH) FC layer (GK) $\rightarrow$ FC layer $\rightarrow$ FC layer
Model 4	(GF) FC layer (MK( $\nu = 0.5$ )) $\rightarrow$ FC layer $\rightarrow$ FC layer
Model 5	FC layer $\rightarrow$ FC layer $\rightarrow$ FC layer

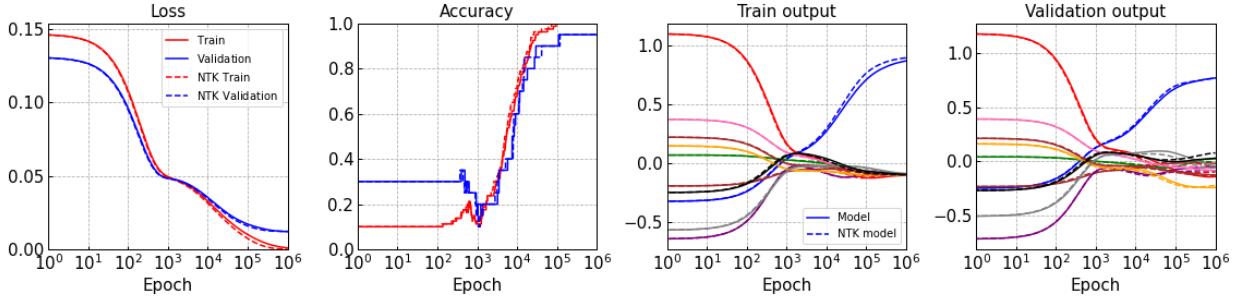


Figure 2: Comparison of SGD/NTK-based methods. Loss/accuracy/output curves for Model 1 with  $\sigma_r = 0.5$  and  $\sigma_s = 0.01$ . In the right two graphs, each color represents an output value when inputting a specific MNIST digit.

## 5.2 Comparison of test loss values for five models

Under the assumption that the width of the layers is infinite, the output  $\mathbf{f}^*$  of the fully trained FCNN is equivalent to the output obtained by NTK regression [25], i.e.,

$$\mathbf{f}^* = \hat{\Theta}_0(\mathbf{x}', \mathcal{X}) \hat{\Theta}_0^{-1} \mathcal{Y}. \quad (14)$$

We investigated the generalization performance in each model by performing NTK regression Eq. (14) using 800 training and 200 validation samples from the MNIST dataset and by computing the loss and the accuracy. The loss is calculated as:

$$\mathcal{L} = \frac{1}{2} |\mathbf{f}^* - \mathbf{y}'|^2, \quad (15)$$

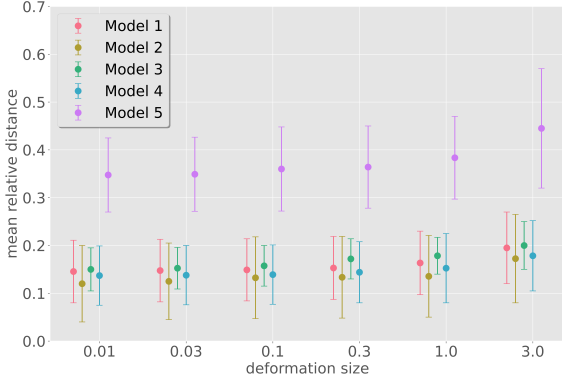
where  $\mathbf{y}'$  is a label of the test data. The results are shown in Tab. 4, where the average of five times and their standard deviations are listed. All models were found to be superior to the conventional models, with Model 4 having the smallest loss and the highest accuracy. The search method for parameters  $\sigma_r$  and  $\sigma_s$  used in the calculations is described in D.3.

## 5.3 Stability to perturbations

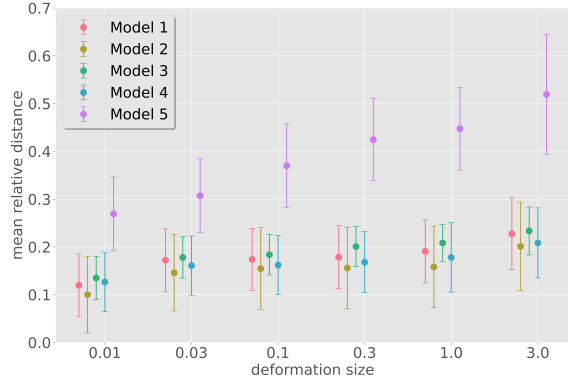
We numerically investigated the robustness of the neural field models to perturbations. The stability of the kernel mapping representation for our models of neural fields was assessed by following the approach of Bietti and Mairal [45]. Fig. 3 shows the mean relative distances for five trials and their standard deviations of a single digit for different deformations or combinations of translations and deformations from the infinite MNIST dataset [48]. The model with a single Gaussian filter and

Table 4: List of test loss values and test accuracy obtained by NTK regression for five models.

	Model 1	Model 2	Model 3	Model 4	Model 5
test loss	$0.0123 \pm 0.0007$	$0.0130 \pm 0.0006$	$0.0121 \pm 0.0004$	$0.0118 \pm 0.0004$	$0.0156 \pm 0.0005$
test accuracy	$90.60 \pm 1.83\%$	$89.80 \pm 1.21\%$	$91.10 \pm 1.39\%$	$93.00 \pm 1.55\%$	$88.90 \pm 1.16\%$



(a) Deformations



(b) Translations and deformations

Figure 3: Average relative distances of single digit for different deformations or combinations of translations and deformations from infinite MNIST dataset [48].

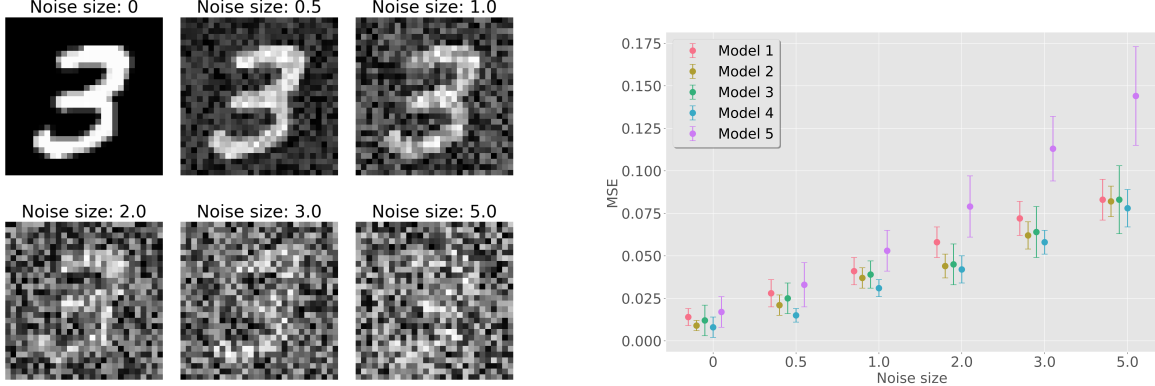
a subsequent MaxPooling layer was most robust to the combinations of random translations and deformations. The Matérn kernel model also exhibited robustness to deformations as well as to combinations of translations and deformations. The search method for parameters  $\sigma_r$  and  $\sigma_s$  used in the calculations is described in D.4. We also evaluated the stability of the neural fields to different levels of noise using the average of five trials and its standard deviation (Figs. 4a and 4b). These results are consistent with our expectations that biologically plausible architectures such as receptive fields and correlations perform some regularization.

## 6 Conclusion

We investigated the behaviors of the supervised learning of RNF locally correlated connections and receptive fields in the NTK regime. We confirmed numerically that neural field models are robust to perturbations of training datasets. A possible mechanism behind this is that the associated RKHSs of neural field models are smaller than those of NTK-parameterized vanilla neural networks. Recently, several works have revealed that vanilla deep neural networks with ReLU activation have the same RKHS as the Laplace kernel [50]. It would be interesting to theoretically identify the RKHS of our neural field models. This paper provides only preliminary results of the supervised learning of neural fields; nevertheless, we believe that it will inspire future studies on neural fields. In particular, we are interested in the analytical justification of NTK governance in the supervised learning of continuum models with a higher dimensionality ( $d \geq 2$ ). Moreover, one can study the effectiveness of the structures in the initial weights further.

## Acknowledgement

This work was supported by JSPS KAKENHI 18K18113 and a grant support from AIST.



(a) Samples from MNIST with different noise levels

(b) MSE loss for different noise levels

Figure 4: Samples from MNIST with stepped noises and the evaluation of robustness of RNFs under different noise levels.

## References

- [1] Shunichi Amari. [Dynamics of Pattern Formation in Lateral-Inhibition Type Neural Fields](#). *Biological Cybernetics*, 27(2):77–87, 1977.
- [2] Teuvo Kohonen. [Self-organized formation of topologically correct feature maps](#). *Biological cybernetics*, 43(1):59–69, 1982.
- [3] A Takeuchi and S Amari. [Formation of Topographic Maps and Columnar Microstructures in Nerve Fields](#). *Biological Cybernetics*, 35(2):63–72, 1979.
- [4] LI Rozonoer. [Random Logical Nets, III](#). *Avtomatika i Telemekhanika*, 7:127–136, 1969.
- [5] Shunichi Amari. [Characteristics of Randomly Connected Threshold-Element Networks and Network Systems](#). *Proceedings of the IEEE*, 59(1):35–47, 1971.
- [6] Shunichi Amari. [Characteristics of Random Nets of Analog Neuron-Like Elements](#). *IEEE Transactions on Systems, Man, and Cybernetics*, 2(5):643–657, 1972.
- [7] Shunichi Amari. [A Method of Statistical Neurodynamics](#). *Kybernetik*, 14(4):201–215, 1974.
- [8] Shunichi Amari, Kiyonori Yoshida, and Kenichi Kanatani. [A Mathematical Foundation for Statistical Neurodynamics](#). *SIAM Journal on Applied Mathematics*, 33(1):95–126, 1977.
- [9] Haim Sompolinsky, Andrea Crisanti, and Hans-Jurgen Sommers. [Chaos in Random Neural Networks](#). *Physical Review Letters*, 61(3):259, 1988.
- [10] Ben Poole, Subhaneil Lahiri, Maithra Raghu, Jascha Sohl-Dickstein, and Surya Ganguli. [Exponential Expressivity in Deep Neural Networks through Transient Chaos](#). In *Advances in Neural Information Processing Systems*, pages 3360–3368, 2016.
- [11] Samuel S. Schoenholz, Justin Gilmer, Surya Ganguli, and Jascha Sohl-Dickstein. [Deep Information Propagation](#). In *International Conference on Learning Representations*, pages 1–18, 2017.

[12] Ryo Karakida, Shotaro Akaho, and Shunichi Amari. [Universal Statistics of Fisher Information in Deep Neural Networks: Mean Field Approach](#). In *Artificial Intelligence and Statistics*, volume 89 of *Proceedings of Machine Learning Research*, pages 1032–1041. PMLR, 2019.

[13] Ryo Karakida, Shotaro Akaho, and Shunichi Amari. [Pathological Spectra of the Fisher Information Metric and Its Variants in Deep Neural Networks](#). *Neural Computation*, 33(8):2274–2307, 2021.

[14] Herbert Jaeger and Harald Haas. Harnessing nonlinearity: Predicting chaotic systems and saving energy in wireless communication. *science*, 304(5667):78–80, 2004.

[15] N Wiener and A Rosenblueth. [The Mathematical Formulation of the Problem of Conduction of Impulses in a Network of Connected Excitable Elements Specifically in Cardiac Muscle](#). *Archivos Del Instituto De Cardiologia De Mexico*, 1:205–265, 1946.

[16] Raymond L Beurle. [Properties of a Mass of Cells Capable of Regenerating Pulses](#). *Philosophical Transactions of the Royal Society of London. Series B, Biological Sciences*, 240:55–94, 1956.

[17] Hugh R Wilson and Jack D Cowan. [Excitatory and Inhibitory Interactions in Localized Populations of Model Neurons](#). *Biophysical Journal*, 12(1):1–24, 1972.

[18] Shunichi Amari. [Learning Patterns and Pattern Sequences by Self-Organizing Nets of Threshold Elements](#). *IEEE Transactions on Computers*, 100(11):1197–1206, 1972.

[19] Hugh R Wilson and Jack D Cowan. [A Mathematical Theory of the Functional Dynamics of Cortical and Thalamic Nervous Tissue](#). *Kybernetik*, 13(2):55–80, 1973.

[20] Olivier Faugeras. [Neural Fields Models of Visual Areas: Principles, Successes, and Caveats](#). In *Computer Vision – ECCV 2012. Workshops and Demonstrations*, pages 474–479. Springer Berlin Heidelberg, 2012.

[21] Stephen Coombes, Peter beim Graben, and Roland Potthast. [Tutorial on Neural Field Theory](#). In *Neural Fields: Theory and Applications*, pages 1–43. Springer, 2014.

[22] Jonathan Touboul. [Propagation of Chaos in Neural Fields](#). *The Annals of Applied Probability*, 24(3):1298–1328, 2014.

[23] Sho Sonoda and Noboru Murata. [Double Continuum Limit of Deep Neural Networks](#). In *ICML 2017 Workshop on Principled Approaches to Deep Learning (PADL)*, volume 1740, pages 1–5, 2017.

[24] Michael Connolly Brady. [A Neural Field Model for Supervised and Unsupervised Learning of the MNIST Dataset](#). In *International Joint Conference on Neural Networks*, pages 1–8. IEEE, 2019.

[25] Arthur Jacot, Franck Gabriel, and Clément Hongler. [Neural Tangent Kernel: Convergence and Generalization in Neural Networks](#). In *Advances in Neural Information Processing Systems*, pages 8571–8580, 2018.

[26] Shun-ichi Amari. [Any Target Function Exists in a Neighborhood of Any Sufficiently Wide Random Network: A Geometrical Perspective](#). *Neural Computation*, 32(8):1431–1447, 2020.

[27] Bo Xie, Yingyu Liang, and Le Song. [Diverse Neural Network Learns True Target Functions](#). In *Artificial Intelligence and Statistics*, pages 1216–1224, 2017.

[28] Lenaic Chizat, Edouard Oyallon, and Francis Bach. [On Lazy Training in Differentiable Programming](#). In *Advances in Neural Information Processing Systems*, pages 1–20, 2018.

[29] Yuanzhi Li and Yingyu Liang. [Learning Overparameterized Neural Networks via Stochastic Gradient Descent on Structured Data](#). In *Advances in Neural Information Processing Systems*, pages 8157–8166, 2018.

[30] Simon S. Du, Xiyu Zhai, Barnabas Poczos, and Aarti Singh. [Gradient Descent Provably Optimizes Over-parameterized Neural Networks](#). In *International Conference on Learning Representations*, pages 1–17, 2019.

[31] Simon S Du, Jason D Lee, Haochuan Li, Liwei Wang, and Xiyu Zhai. [Gradient Descent Finds Global Minima of Deep Neural Networks](#). In *Proceedings of the 36th International Conference on Machine Learning*, volume 97, pages 1675–1685, 2019.

[32] Jaehoon Lee, Lechao Xiao, Samuel S Schoenholz, Yasaman Bahri, Jascha Sohl-Dickstein, and Jeffrey Pennington. [Wide Neural Networks of Any Depth Evolve as Linear Models Under Gradient Descent](#). In *Advances in Neural Information Processing Systems*, pages 8572–8583, 2019.

[33] Sanjeev Arora, Simon S Du, Hu Wei, Zhiyuan Li, Ruslan Salakhutdinov, and Ruosong Wang. [On Exact Computation with an Infinitely Wide Neural Net](#). In *Advances in Neural Information Processing Systems*, pages 8139–8148, 2019.

[34] Zeyuan Allen-Zhu, Yuanzhi Li, and Yingyu Liang. [Learning and Generalization in Overparameterized Neural Networks, Going Beyond Two Layers](#). In *Advances in Neural Information Processing Systems*, pages 6155–6166, 2019.

[35] Sanjeev Arora, Simon S Du, Wei Hu, Zhiyuan Li, and Ruosong Wang. [Fine-Grained Analysis of Optimization and Generalization for Overparameterized Two-Layer Neural Networks](#). In *36th International Conference on Machine Learning*, pages 477–502, 2019.

[36] Greg Yang. [Scaling Limits of Wide Neural Networks with Weight Sharing: Gaussian Process Behavior, Gradient Independence, and Neural Tangent Kernel Derivation](#). *arXiv preprint arXiv:1902.04760*, 2019.

[37] Yuan Cao and Quanquan Gu. [Generalization Bounds of Stochastic Gradient Descent for Wide and Deep Neural Networks](#). In *Advances in Neural Information Processing Systems*, pages 10835–10845, 2019.

[38] Difan Zou, Yuan Cao, Dongruo Zhou, and Quanquan Gu. [Gradient Descent Optimizes Over-parameterized Deep ReLU Networks](#). *Machine Learning*, 109:467–492, 2020.

[39] Marlene R Cohen and Adam Kohn. [Measuring and Interpreting Neuronal Correlations](#). *Nature Neuroscience*, 14(7):811, 2011.

[40] Alberto Bietti and Julien Mairal. [Group Invariance, Stability to Deformations, and Complexity of Deep Convolutional Representations](#). *The Journal of Machine Learning Research*, 20(1): 876–924, 2019.

[41] Paul C Bressloff. [Spatiotemporal Dynamics of Continuum Neural Fields](#). *Journal of Physics A: Mathematical and Theoretical*, 45(3):033001, 2011.

[42] James Rankin, Daniele Avitabile, Javier Baladron, Gregory Faye, and David JB Lloyd. [Continuation of Localized Coherent Structures in Nonlocal Neural Field Equations](#). *SIAM Journal on Scientific Computing*, 36(1):B70–B93, 2014.

[43] David Marr. [Vision: A Computational Investigation into the Human Representation and Processing of Visual Information](#). Inc., New York, NY, 2(4.2), 1982.

[44] Takeyuki Hida. [Canonical Representations of Gaussian Processes and Their Applications](#). *Memoirs of the College of Science, University of Kyoto. Series A: Mathematics*, 33(1):109–155, 1960.

[45] Alberto Bietti and Julien Mairal. [On the Inductive Bias of Neural Tangent Kernels](#). In *Advances in Neural Information Processing Systems*, pages 12873–12884, 2019.

[46] Yann LeCun, Léon Bottou, Yoshua Bengio, and Patrick Haffner. [Gradient-Based Learning Applied to Document Recognition](#). *Proceedings of the IEEE*, 86(11):2278–2324, 1998.

[47] Roman Novak, Lechao Xiao, Jaehoon Lee, Yasaman Bahri, Greg Yang, Jiri Hron, Daniel A Abolafia, Jeffrey Pennington, and Jascha Sohl-Dickstein. [Bayesian Deep Convolutional Networks with Many Channels Are Gaussian Processes](#). In *International Conference on Learning Representations*, pages 1–35, 2019.

[48] Gaëlle Loosli, Stéphane Canu, and Léon Bottou. [Training Invariant Support Vector Machines using Selective Sampling](#). *Large Scale Kernel Machines*, 2, 2007.

[49] Andrew M. Saxe, Pang Wei Koh, Zhenghao Chen, Maneesh Bhand, Bipin Suresh, and Andrew Y. Ng. [On Random Weights and Unsupervised Feature Learning](#). In *28th International Conference on Machine Learning*, pages 1089–1096, 2011.

[50] Lin Chen and Sheng Xu. [Deep Neural Tangent Kernel and Laplace Kernel Have the Same RKHS](#). In *International Conference on Learning Representations*, pages 1–22, 2021.

[51] Viacheslav Borovitskiy, Alexander Terenin, Peter Mostowsky, and Marc Peter Deisenroth. [Matérn Gaussian processes on Riemannian manifolds](#). In *Advances in Neural Information Processing Systems (NeurIPS)*, pages 12426–12437, 2020.

## A Matérn Kernel and RBF Kernel on $\mathbb{T}^d$

The formulations of the Matérn kernel and RBF kernel on the  $d$ -dimensional torus  $\mathbb{T}^d$  are given as follows [51]:

$$K_\nu(\mathbf{z}_{l-1}, \mathbf{z}'_{l-1}) = \sum_{\mathbf{n} \in \mathbb{Z}^d} \frac{2^{1-\nu}}{C_\nu \Gamma(\nu)} \left( \frac{\sqrt{2\nu} |\mathbf{z}_{l-1} - \mathbf{z}'_{l-1} + \mathbf{n}|}{\sigma_{s_{l-1}}} \right)^\nu B_\nu \left( \frac{\sqrt{2\nu} |\mathbf{z}_{l-1} - \mathbf{z}'_{l-1} + \mathbf{n}|}{\sigma_{s_{l-1}}} \right), \quad (16)$$

$$K_\infty(\mathbf{z}_{l-1}, \mathbf{z}'_{l-1}) = \sum_{\mathbf{n} \in \mathbb{Z}^d} \frac{1}{C_\infty} \exp \left( -\frac{|\mathbf{z}_{l-1} - \mathbf{z}'_{l-1} + \mathbf{n}|^2}{2\sigma_{s_{l-1}}^2} \right), \quad (17)$$

respectively, where  $\mathbf{z}_l$  and  $\mathbf{z}'_{l-1}$  are the positions of neurons in the  $(l-1)$ th layer,  $C_\nu$  is a constant to ensure  $K_\nu(\mathbf{z}, \mathbf{z}) = 1$ ,  $B_\nu(\cdot)$  is a modified Bessel function of the second kind,  $\sigma_{s_{l-1}} \in \mathbb{R}_+$  is a scaling parameter that indicates the degree of the correlation of neurons in the  $(l-1)$ th layer, and  $\nu \in \mathbb{R}_+$  is a parameter that represents the smoothness of a function generated by the Gaussian process.

## B Justification of White Noise

It is known that white noise is non-differentiable everywhere from the Paley–Wiener–Zygmund theorem. That is, white noise is not Riemann integrable and thus the convolution is not well-defined. In this appendix, we describe how to justify white noise using the generalized function theory of infinite variables.

We consider real-valued function  $\xi : \mathbb{R} \rightarrow \mathbb{R}$ , which satisfies the following conditions.

- $\xi$  is a  $C^\infty$  function.
- For any non-negative integers  $m$  and  $n$ ,  $\sup_x \left| x^m \frac{d^m}{dx^m} \xi(x) \right| < \infty$  is satisfied.

In this case,  $\xi$  is called a rapidly decreasing function on  $\mathbb{R}$ , and the whole of the rapidly decreasing function on  $\mathbb{R}$  is denoted by  $\mathcal{S}(\mathbb{R})$ , which is called the Schwartz space. The whole of the continuous linear functionals on  $\mathcal{S}(\mathbb{R})$  is represented by  $\mathcal{S}'(\mathbb{R})$ , where the elements of  $\mathcal{S}'(\mathbb{R})$  are Schwartz's generalized functions. We use the standard bilinear form  $b(x, \xi)$  on  $\mathcal{S}'(\mathbb{R}) \times \mathcal{S}(\mathbb{R})$  for descriptive simplicity. If  $f(t)$  is a rapidly decreasing function, then by

$$b(x_f, \xi) = \int_{\mathbb{R}} f(t) \xi(t) dt, \quad (18)$$

$x_f$  is a continuous linear functional on  $\mathcal{S}(\mathbb{R})$ , that is, it is a generalized function. Since function  $f$  defines one generalized function, the Gelfand triple

$$\mathcal{S}(\mathbb{R}) \subset L^2(\mathbb{R}) \subset \mathcal{S}'(\mathbb{R}), \quad (19)$$

of the inclusion relation in the function space holds.

$\mathcal{S}'(\mathbb{R})$  introduces a probability measure,  $\mu$ , that is uniquely determined by

$$\int_{\mathcal{S}'(\mathbb{R})} \exp(ib(x, \xi)) \mu(dx) = \exp\left(-\frac{b(\xi, \xi)}{2}\right). \quad (20)$$

This is called the Gaussian measure, and the probability space  $(\mathcal{S}'(\mathbb{R}), \mu)$  is called the Gaussian space. If we fix  $\xi \in \mathcal{S}(\mathbb{R})$  and set

$$x \mapsto X_\xi(x) = b(x, \xi), \quad (21)$$

then  $X_\xi$  is a function on  $\mathcal{S}'(\mathbb{R})$ ; that is, a random variable defined on  $(\mathcal{S}'(\mathbb{R}), \mu)$ . Now,  $X_\xi$  is a Gaussian family with mean 0 and covariance

$$\mathbb{E}[X_\xi X_\eta] = b(\xi, \eta), \quad \xi, \eta \in \mathcal{S}(\mathbb{R}). \quad (22)$$

We recognize that

$$X(f) = \int_{\mathbb{R}} f(t) W(t) dt \quad (23)$$

is a Gaussian random variable for function  $f(t)$  that guarantees that  $B(t)$  is a Gaussian process.  $X(f)$  is a Gaussian family with mean 0 and covariance  $\text{Cov}[X(f), X(g)] = b(f, g)$ .

Now, let

$$X_\xi(x) = b(x, \xi) = \int_{\mathbb{R}} x(t) \xi(t) dt \quad (24)$$

be the integral representation of Eq.(21), and if we compare with Eq.(23), we can represent it as  $w(t) = x(t) = b(x, \delta_t)$ .

The whole sequence of functions  $\phi = (f_n)_{n=0}^{\infty}$ ,  $f_n \in L^2(\mathbb{R}^n)_{\text{sym}}$  satisfying

$$\|\phi\|^2 = \sum_{n=0}^{\infty} n! |f_n|^2 < \infty \quad (25)$$

forms a Hilbert space. This is called the Boson Fock space on  $L^2(\mathbb{R})$ , which is denoted by  $\Gamma(L^2(\mathbb{R}))$ . For any  $\xi \in \mathcal{S}(\mathbb{R})$ , the corresponding  $\varphi_{\xi} \in L^2(\mathcal{S}'(\mathbb{R}), \mu)$ , and  $(1, \xi, \xi^{\otimes 2}/2!, \dots, \xi^{\otimes n}/n!) \in \Gamma(L^2(\mathbb{R}))$  defined in

$$\varphi_{\xi}(x) = \exp\left(\frac{b(x, \xi) - b(\xi, \xi)}{2}\right), \quad x \in \mathcal{S}'(\mathbb{R}), \quad (26)$$

we obtain the unitary isomorphism  $L^2(\mathcal{S}'(\mathbb{R}), \mu) \cong \Gamma(L^2(\mathbb{R}))$  with the Wiener–Itô–Segal isomorphism.

If we apply the Wiener–Itô–Segal isomorphism to the Gelfand triplet

$$\Gamma(\mathcal{S}(\mathbb{R})) \subset \Gamma(L^2(\mathbb{R})) \subset \Gamma(\mathcal{S}'(\mathbb{R})), \quad (27)$$

we have the inclusion relation

$$\mathcal{W} \subset L^2(\mathcal{S}'(\mathbb{R}), \mu) \subset \mathcal{W}' \quad (28)$$

of the function space on the Gaussian space. This is a Gelfand triplet in Gaussian space; the elements of  $\mathcal{W}'$  are generalized functions in Gaussian space, and this becomes the generalized function of white noise. By referring to it as white noise, the following holds.

**Theorem B.1.** *The Wiener process  $t \mapsto B(t) \in \mathcal{W}'$  and white noise  $t \mapsto W(t) \in \mathcal{W}'$  are both  $C^\infty$ , and*

$$\frac{d}{dt} B(t) = W(t) \quad (29)$$

holds on  $\mathcal{W}'$ .

This theorem shows that white noise is differentiable everywhere and that the convolution is well-defined.

## C Discretization and Correlations

### C.1 Proof of Proposition 1 (decomposition of covariance matrix)

*Proof.* For any measurable set of Euclidean space  $E$ ,

$$P(Y \in E) = \int_E (2\pi)^{-d/2} \exp\left(-\frac{|\mathbf{y}|^2}{2}\right) d\mathbf{y} \quad (30)$$

$$= \int_{A(E)} (2\pi)^{-d/2} \exp\left(-\frac{|A^{-1}\mathbf{x}|^2}{2}\right) \left|\frac{\partial \mathbf{y}}{\partial \mathbf{x}}\right| d\mathbf{x} \quad (31)$$

$$= \int_{A(E)} (2\pi)^{-d/2} |A|^{-1} \exp\left(-\frac{\mathbf{x}^\top (AA^\top)^{-1}\mathbf{x}}{2}\right) d\mathbf{x} \quad (32)$$

where we use  $|A^{-1}\mathbf{x}|^2 = \mathbf{x}^\top (A^{-1})^\top A^{-1}\mathbf{x}$  and  $|\partial \mathbf{y} / \partial \mathbf{x}| = |A^{-1}| = |A|^{-1}$ . Thus, if we have  $\Sigma = AA^\top$  for some  $A$ , then  $X \sim \mathcal{N}(\mathbf{0}_d, \Sigma)$ .  $\square$

## C.2 Decomposition of covariance

Consider the system

$$\Sigma(\mathbf{x}, \mathbf{y}) = \int_{\mathbb{R}^d} A(\mathbf{x}, \mathbf{z}) A^*(\mathbf{z}, \mathbf{y}) d\mathbf{z} = f(\mathbf{x} - \mathbf{y}), \quad \mathbf{x}, \mathbf{y} \in \mathbb{R}^d. \quad (33)$$

We assume that  $f$  is a real even function and that  $A(\mathbf{x}, \mathbf{y}) = g(\mathbf{x} - \mathbf{y})$  for some real even function  $g$ . Then,  $A^*(\mathbf{x}, \mathbf{y}) = g^*(\mathbf{x} - \mathbf{y}) = g(\mathbf{y} - \mathbf{x})$ , and

$$\begin{aligned} \int_{\mathbb{R}^d} A(\mathbf{x}, \mathbf{z}) A^*(\mathbf{y}, \mathbf{z}) d\mathbf{z} &= \int_{\mathbb{R}^d} g(\mathbf{x} - \mathbf{z}) g(\mathbf{y} - \mathbf{z}) d\mathbf{z} \\ &= \int_{\mathbb{R}^d} g(\mathbf{z}) g(\mathbf{y} - \mathbf{x} + \mathbf{z}) d\mathbf{z} \\ &= \int_{\mathbb{R}^d} g(\mathbf{z}) g((\mathbf{x} - \mathbf{y}) - \mathbf{z}) d\mathbf{z} \\ &= (g * g)(\mathbf{x} - \mathbf{y}). \end{aligned} \quad (34)$$

Thus, Eq.(33) is reduced to

$$(g * g)(\mathbf{x} - \mathbf{y}) = f(\mathbf{x} - \mathbf{y}), \quad \mathbf{x}, \mathbf{y} \in \mathbb{R}^d. \quad (35)$$

By taking the Fourier transform in  $\mathbf{x}$ , we obtain

$$\hat{g}^2(\boldsymbol{\xi}) = \hat{f}(\boldsymbol{\xi}) = \int_{\mathbb{R}^d} f(\mathbf{x}) \exp(-i\mathbf{x} \cdot \boldsymbol{\xi}) d\mathbf{x}, \quad \boldsymbol{\xi} \in \mathbb{R}^d, \quad (36)$$

where  $\mathbf{x} \cdot \boldsymbol{\xi}$  represents the dot product of  $\mathbf{x}$  and  $\boldsymbol{\xi}$ . Therefore,  $g(\mathbf{x})$  can be represented as

$$g(\mathbf{x}) = \mathcal{F}^{-1} \left[ \sqrt{\hat{f}(\boldsymbol{\xi})} \right] = (2\pi)^{-d} \int_{\mathbb{R}^d} \sqrt{\hat{f}(\boldsymbol{\xi})} \exp(i\boldsymbol{\xi} \cdot \mathbf{x}) d\boldsymbol{\xi}, \quad \boldsymbol{\xi} \in \mathbb{R}^d, \quad (37)$$

where  $\mathcal{F}^{-1}$  is a Fourier inverse transform.

## C.3 Case of Gaussian kernel

$f(\mathbf{x})$  and  $\hat{f}(\boldsymbol{\xi})$  are given as:

$$f(\mathbf{x}) = \exp \left( -\frac{|\mathbf{x}|^2}{2\sigma_s^2} \right), \quad \mathbf{x} \in \mathbb{R}^d \quad (38)$$

$$\hat{f}(\boldsymbol{\xi}) = (2\pi)^{d/2} \sigma_s^d \exp \left( -\frac{\sigma_s^2 |\boldsymbol{\xi}|^2}{2} \right), \quad \boldsymbol{\xi} \in \mathbb{R}^d. \quad (39)$$

Substituting Eq.(39) into Eq.(37), we obtain

$$g(\mathbf{x}) = \mathcal{F}^{-1} \left[ \sqrt{\hat{f}(\boldsymbol{\xi})} \right] \quad (40)$$

$$= \mathcal{F}^{-1} \left[ (2\pi)^{d/4} \sigma_s^{d/2} \exp \left( -\frac{(\sigma_s^2/2)|\boldsymbol{\xi}|^2}{2} \right) \right] \quad (41)$$

$$= \frac{2^{d/2}}{\sigma_s^{d/2} (2\pi)^{d/4}} \mathcal{F}^{-1} \left[ (2\pi)^{d/2} \left( \frac{\sigma_s}{\sqrt{2}} \right)^d \exp \left( -\frac{(\sigma_s/\sqrt{2})^2 |\boldsymbol{\xi}|^2}{2} \right) \right] \quad (42)$$

$$= \left( \frac{2}{\pi \sigma_s^2} \right)^{d/4} \exp \left( -\frac{|\mathbf{x}|^2}{\sigma_s^2} \right), \quad (43)$$

and thus,

$$A(\mathbf{x}, \mathbf{y}) = g(\mathbf{x} - \mathbf{y}) = \left( \frac{2}{\pi \sigma_s^2} \right)^{d/4} \exp \left( -\frac{|\mathbf{x} - \mathbf{y}|^2}{\sigma_s^2} \right). \quad (44)$$

By using white noise  $W(\mathbf{x})$  with  $\sigma^2 = 1$  on  $\mathbb{R}^d$  with

$$S(\mathbf{x}) := (AW(\mathbf{x})) = \left( \frac{2}{\pi \sigma_s^2} \right)^{d/4} \int_{\mathbb{R}^d} \exp \left( -\frac{|\mathbf{x} - \mathbf{y}|^2}{\sigma_s^2} \right) W(\mathbf{y}) d\mathbf{y}, \quad (45)$$

we obtain

$$\mathbb{E}[S(\mathbf{x})] \equiv 0 \quad (46)$$

$$\mathbb{E}[S(\mathbf{x})S(\mathbf{y})] = f(\mathbf{x} - \mathbf{y}) = \exp \left( -\frac{|\mathbf{x} - \mathbf{y}|^2}{\sigma_s^2} \right), \quad (47)$$

and  $S(\mathbf{x})$  is a Gaussian process with  $f(\mathbf{x} - \mathbf{y})$  as its covariance. Since the model used in this study is 1-RNF, we consider the case of  $d = 1$ . Let the continuous variables be  $x, y \in \mathbb{R}$ , and discretize them into discrete variables  $i$  and  $j$ , which are elements of the  $n$ -dimensional vector. We replace each of them according to the following rules.

$$x_i := \frac{1}{n} \left( i - \frac{n}{2} \right), \quad i \in [n] \quad (48)$$

$$y_i := \frac{1}{n} \left( j - \frac{n}{2} \right), \quad j \in [n]. \quad (49)$$

For simplicity of description, the symbols

$$\Delta x := (x_{i+1} - x_i) = \frac{1}{n} \quad (50)$$

$$\Delta y := (y_{i+1} - y_i) = \frac{1}{n} \quad (51)$$

are introduced. Now, the relation

$$f(x - x') = \int_{\mathbb{R}} g(x - y)g(x' - y) dy, \quad \forall x, x' \in \mathbb{R}, \quad (52)$$

where

$$f(x) = \exp \left( -\frac{x^2}{2\sigma_s^2} \right) \quad (53)$$

$$g(x) = \left( \frac{2}{\pi \sigma_s^2} \right)^{1/4} \exp \left( -\frac{x^2}{\sigma_s^2} \right), \quad (54)$$

holds from the discussion of the continuous system. We obtain the decomposition of the covariance matrix  $\Sigma = AA^T$  using Eq.(52). By using the partitioning quadrature method, we obtain

$$f(x - x') \approx \sum_{j=1}^n g(x - y_j)g(x' - y_j)\Delta y, \quad \forall x, x' \in \mathbb{R}. \quad (55)$$

Here, the covariance matrix  $\Sigma$  and the transformation matrix  $A$  are defined by  $f$  as:

$$\Sigma_{ii'} = f(x_i - x_{i'}) \quad (56)$$

$$= \exp\left(-\frac{|x_i - x_{i'}|^2}{2\sigma_s^2}\right) \quad (57)$$

$$= \exp\left(-\frac{|i - i'|^2}{2(\sigma_s/\Delta x)^2}\right) \quad (58)$$

$$A_{ij} = g(x_i - y_j) \sqrt{\Delta y} \quad (59)$$

$$= \left(\frac{2}{\pi\sigma_s^2}\right)^{1/4} (\Delta y)^{1/4} \exp\left(-\frac{|x_i - y_j|^2}{\sigma_s^2}\right) \quad (60)$$

$$= \left(\frac{2}{\pi(\sigma_s/\Delta y)^2}\right)^{1/4} \exp\left(-\frac{|i - j|^2}{(\sigma_s/\Delta y)^2}\right), \quad (61)$$

where  $\Delta x = \Delta y$ . From Eqs.(58) and (61), we obtain

$$\Sigma_{ii'} \approx \sum_{j=1}^n A_{ij} A_{i'j}, \quad \forall i, i'. \quad (62)$$

That is,  $\Sigma \approx AA^\top$  holds.

#### C.4 Case of Matérn kernel

In the case of the Matérn kernel, the normal Fourier transform of a radial function is not possible. We transform it using the following theorem.

**Theorem C.1.** *Let  $r = |\mathbf{x}|$  and  $s = |\boldsymbol{\xi}|$ , and write  $f(\mathbf{x}) = F(r)$  and  $\hat{f}(\boldsymbol{\xi}) = \hat{F}_d(s)$ . The radial Fourier transform in  $d$ -dimensions is given in terms of the Hankel transform by*

$$s^{\frac{d}{2}-1} \hat{F}_d(s) = (2\pi)^{\frac{d}{2}} \int_0^\infty J_{\frac{d}{2}-1}(sr) r^{\frac{d}{2}-1} F(r) r dr, \quad (63)$$

where  $J_\nu(\cdot)$  is a Bessel function of the first kind.

The Matérn kernel is represented by the following equation:

$$f(\mathbf{x}) = \frac{2^{1-\nu}}{\Gamma(\nu)} \left(\frac{\sqrt{2\nu}|\mathbf{x}|}{\theta}\right)^\nu B_\nu\left(\frac{\sqrt{2\nu}|\mathbf{x}|}{\theta}\right). \quad (64)$$

By using this theorem to perform the transformation, we obtain

$$\hat{f}(\boldsymbol{\xi}) = \hat{F}_d(s) = s^{-\frac{d}{2}+1} (2\pi)^{\frac{d}{2}} \int_0^\infty J_{\frac{d}{2}-1}(sr) r^{\frac{d}{2}-1} F(r) r dr \quad (65)$$

$$= \frac{\Gamma\left(\frac{d}{2} + \nu\right)}{\Gamma(\nu)} \frac{(2\theta)^d (2\nu)^\nu \pi^{\frac{d}{2}}}{(s^2\theta^2 + 2\nu)^{\frac{d}{2} + \nu}}. \quad (66)$$

When  $d > 1$ , the equations and calculations become very complex; hence, we will consider the case of  $d = 1$  in accordance with the 1-RNF of the model used. In the case of  $d = 1$ , we obtain

$$\hat{f}(\boldsymbol{\xi}) = \frac{\Gamma\left(\nu + \frac{1}{2}\right)}{\Gamma(\nu)} \frac{2\theta(2\nu)^\nu \sqrt{\pi}}{(\xi^2\theta^2 + 2\nu)^{\nu + \frac{1}{2}}}. \quad (67)$$

Substituting Eq.(67) into Eq.(37), we obtain

$$g(x) = \mathcal{F}^{-1} \left[ \sqrt{\hat{f}(\xi)} \right] \quad (68)$$

$$= \frac{1}{\sqrt{\pi\theta\Gamma(2\nu)}} \left( \frac{|x|}{\theta} \right)^\nu B_\nu \left( \frac{\sqrt{2\nu}|x|}{\theta} \right), \quad (69)$$

and thus

$$A(x, y) = g(x - y) = \frac{1}{\sqrt{\pi\theta\Gamma(2\nu)}} \left( \frac{|x - y|}{\theta} \right)^\nu B_\nu \left( \frac{\sqrt{2\nu}|x - y|}{\theta} \right). \quad (70)$$

Following the argument in C.3, we obtain

$$\Sigma_{ii'} = f(x_i - x_{i'}) \quad (71)$$

$$= \frac{2^{1-\nu}}{\Gamma(\nu)} \left( \frac{\sqrt{2\nu}|x_i - x_{i'}|}{\theta} \right)^\nu B_\nu \left( \frac{\sqrt{2\nu}|x_i - x_{i'}|}{\theta} \right) \quad (72)$$

$$= \frac{2^{1-\nu}}{\Gamma(\nu)} \left( \frac{\sqrt{2\nu}|i - i'|\Delta x}{\theta} \right)^\nu B_\nu \left( \frac{\sqrt{2\nu}|i - i'|\Delta x}{\theta} \right) \quad (73)$$

$$A_{ij} = g(x_i - y_j) \sqrt{\Delta y} \quad (74)$$

$$= \frac{1}{\sqrt{\pi\theta\Gamma(2\nu)}} \left( \frac{|x_i - y_j|}{\theta} \right)^\nu B_\nu \left( \frac{\sqrt{2\nu}|x_i - y_j|}{\theta} \right) \sqrt{\Delta y} \quad (75)$$

$$= \sqrt{\frac{\Delta y}{\pi\theta\Gamma(2\nu)}} \left( \frac{|(i - j)\Delta y|}{\theta} \right)^\nu B_\nu \left( \frac{\sqrt{2\nu}|(i - j)\Delta y|}{\theta} \right). \quad (76)$$

## D Further Experimental Details

### D.1 Visualization of initial weight matrix

We visualized the initial weight matrix from the input layer to the first hidden layer of each model defined in Tab. 3. Figs. 5.(a), (b), and (c) show how the receptive field shrinks as  $\sigma_r$  is decreased. In Fig. 5.(d), the receptive field is a Mexican hat, and the figure shows the inhibitory property as defined. In Fig. 5.(e), the Mate n kernel is used to correlate between neurons when generating weights, resulting in a difference in distribution. Fig. 5.(f) shows the NTK parameterization, where the weights are generated from a standard Gaussian distribution.

### D.2 Other models in the NTK regime

We confirm that Models 2, 3, 4, and 5 are also in the NTK regime (Fig. 6).

### D.3 Calculating loss by NTK regression with different combinations of $\sigma_r$ and $\sigma_s$

To verify the validity of the obtained values, the five-time averages of the loss values and their standard deviations were calculated.

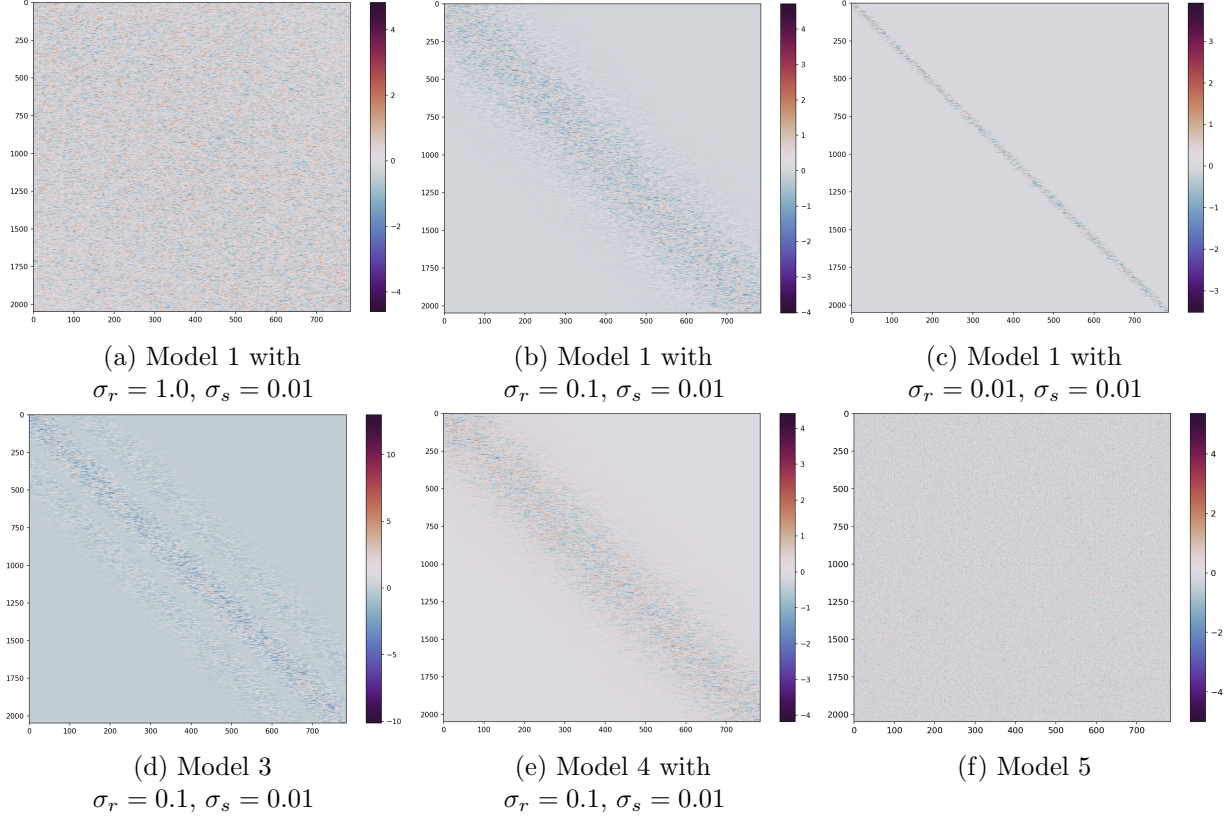
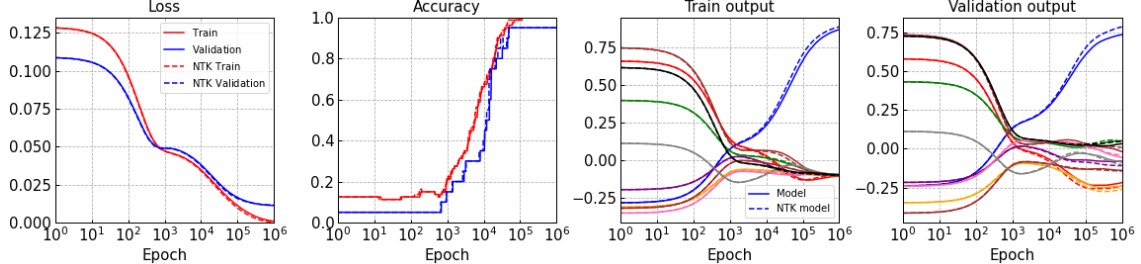


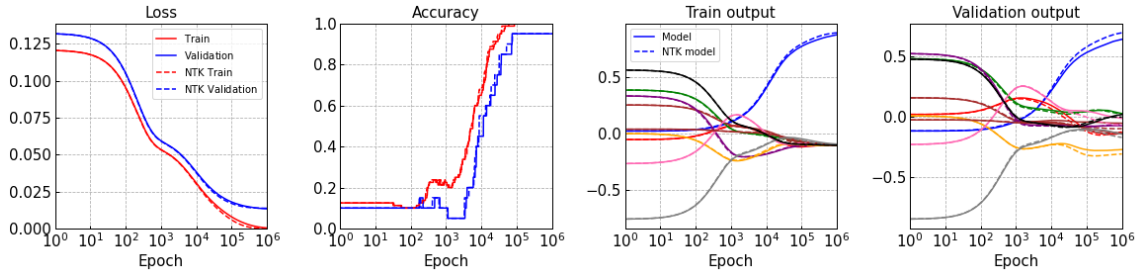
Figure 5: Initial weight matrix from input layer to first hidden layer. Color bar on right indicates weight values.

#### D.4 Average relative distances with different combinations of $\sigma_r$ and $\sigma_s$

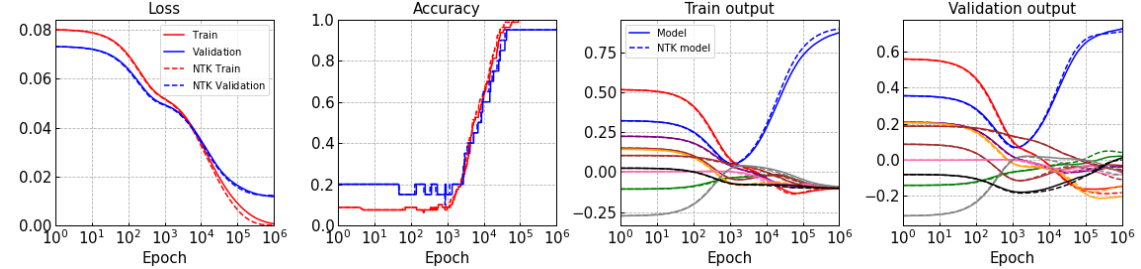
To obtain the optimal parameters  $\sigma_r$  and  $\sigma_s$  that minimize average relative distances to translations and deformations, a parameter search is performed.



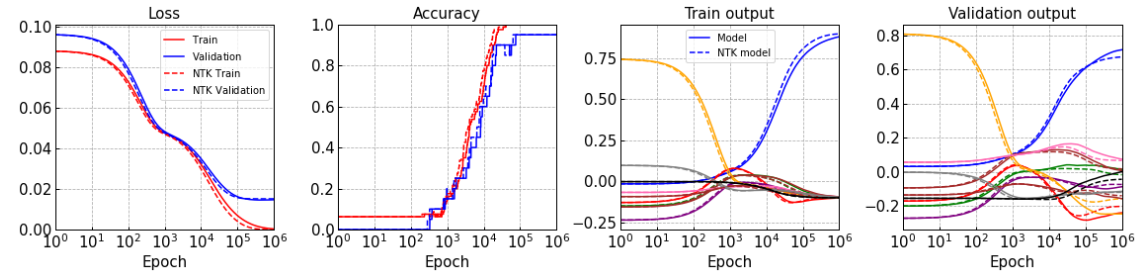
(a) Comparison of SGD/NTK-based loss/accuracy/output curves for Model 2 with  $\sigma_r = 0.5$  and  $\sigma_s = 0.01$ .



(b) Comparison of SGD/NTK-based loss/accuracy/output curves for Model 3 with  $\sigma_r = 0.01$  and  $\sigma_s = 0.01$ .



(c) Comparison of SGD/NTK-based loss/accuracy/output curves for Model 4 with  $\sigma_r = 0.5$  and  $\sigma_s = 0.01$ .



(d) Comparison of SGD/NTK-based loss/accuracy/output curves for Model 5.

Figure 6: Comparison of SGD/NTK-based loss/accuracy/output curves for five models.

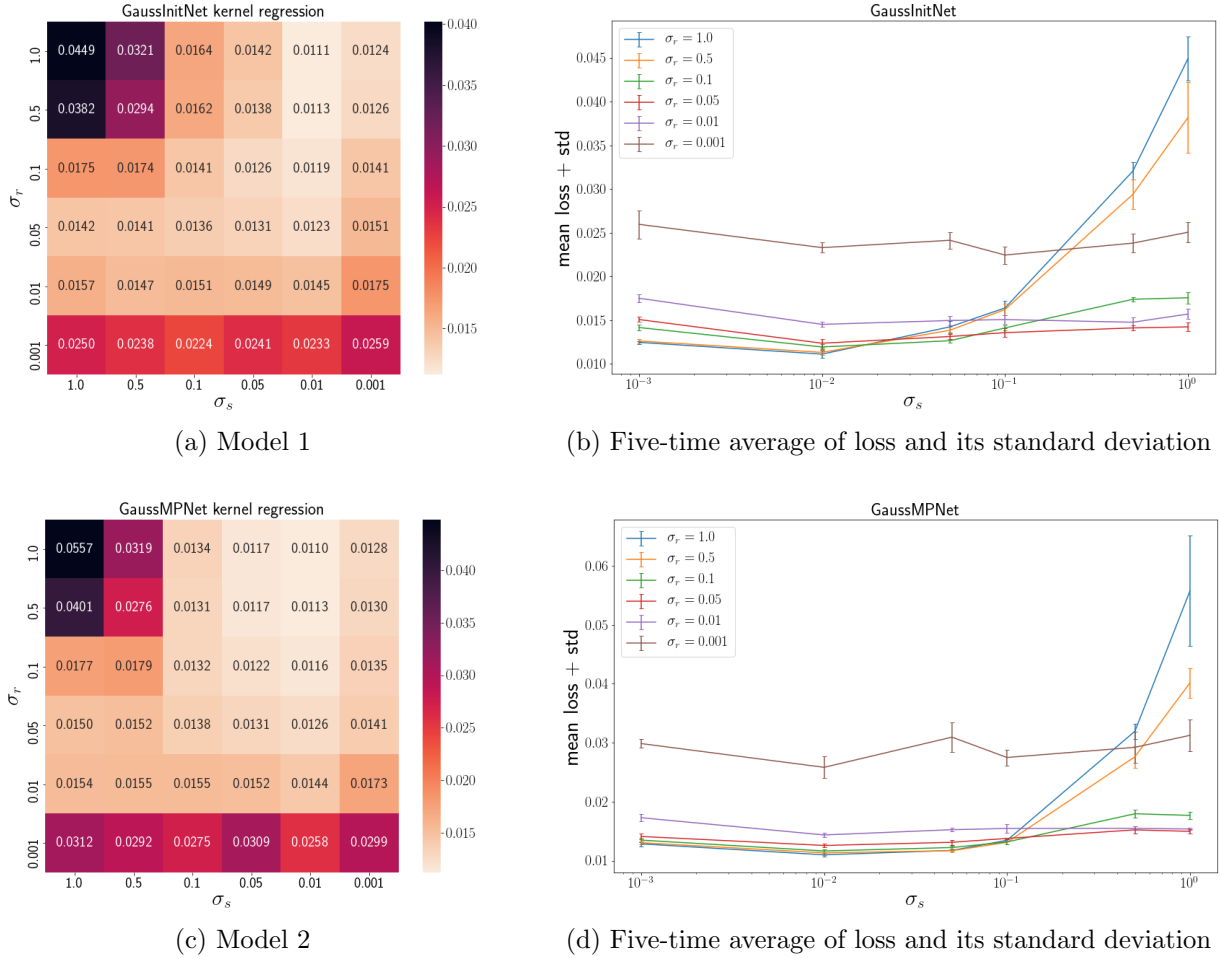


Figure 7: Heatmaps of losses for Model 1 and Model 2, and five-time average and standard deviations of losses with different combinations of  $\sigma_r$  and  $\sigma_s$ .

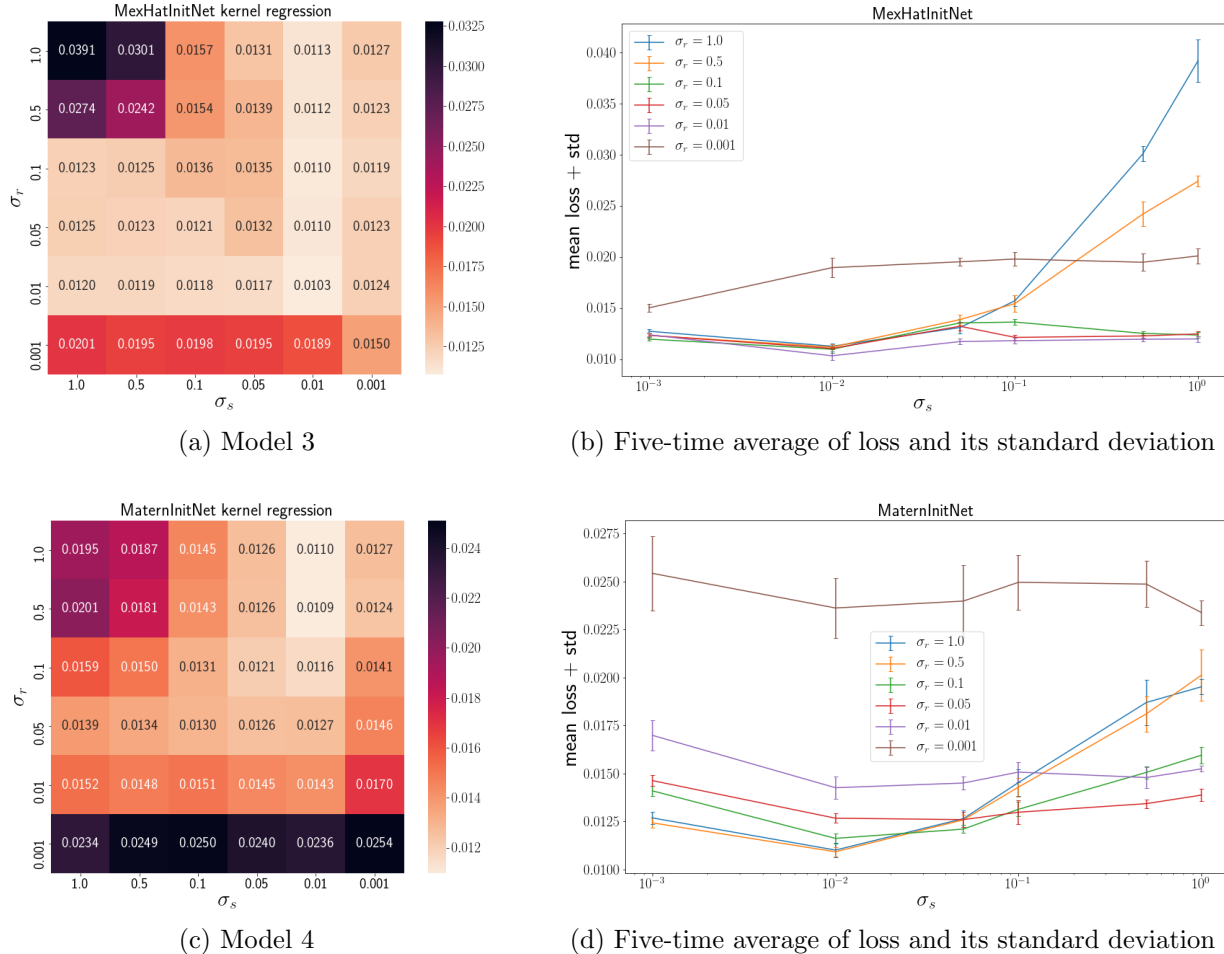


Figure 8: Heatmaps of losses for Model 3 and Model 4, and five-time average and standard deviations of losses with different combinations of  $\sigma_r$  and  $\sigma_s$ .



Figure 9: Average relative distances to deformations with different combinations of  $\sigma_r$  and  $\sigma_s$ .

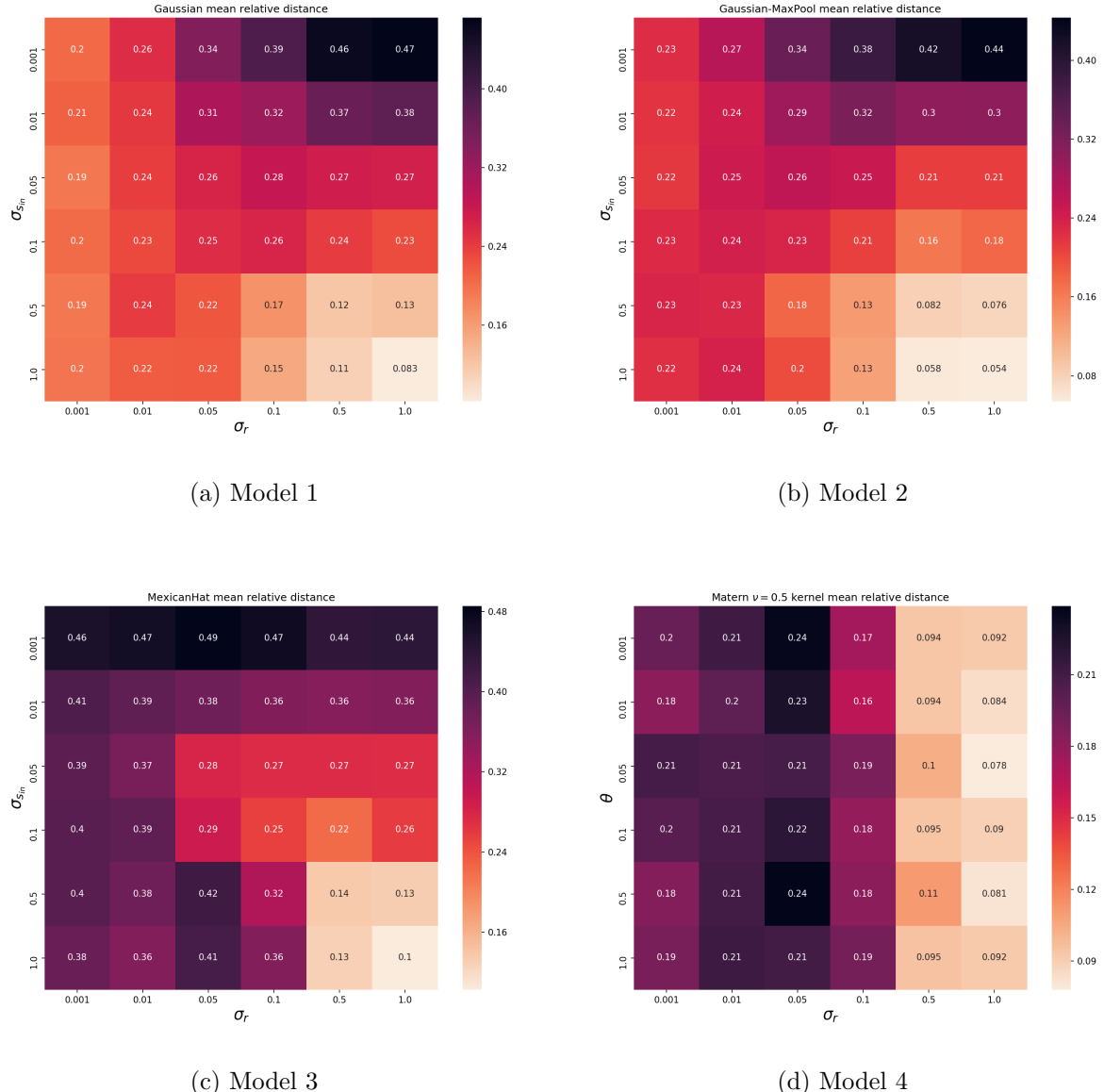


Figure 10: Average relative distances to translations and deformations with different combinations of  $\sigma_r$  and  $\sigma_s$ .